

Intramolecular Charge Transfer in Ruthenium Complexes [Ru(acac)₂(ciq)] with Ambidentate Camphoriminoquinone (ciq) Ligands

Vasileios Filippou,^[a] Svenja Bickle,^[a] Martina Bubrin,^[a] and Wolfgang Kaim*^[a]

Dedicated to Professor Christoph Janiak on the Occasion of his 60th Birthday

Reaction of [Ru(acac)₂(MeCN)₂], acac⁻=acetylacetone, with *N*-phenylcamphoriminoquinone (pciq) or the new *N*-(2-thiomethylphenyl)-camphoriminoquinone (tciq) produces complexes [Ru(acac)₂(pciq)] and [Ru(acac)₂(tciq)] with N,O or N,S coordination and *E* or *Z* configuration at the C=N bond, respectively. Oxidation state assignments in comparison with classical

iminoquinone ligands are based on structural data in connection with DFT calculations. Reversible oxidation yields complex ions [Ru^{III}(acac)₂(pciq)]⁺ and [Ru^{III}(acac)₂(tciq)]⁺ as characterized by EPR, IR and UV-vis-NIR spectroelectrochemistry.

Introduction

N,O-Chelating *o*-iminoquinone/*o*-iminosemiquinone/*o*-amido-phenolate redox systems involving radical intermediates such as ISQ (Figure 1) have played an important role in the analysis and understanding of noninnocent ligand behavior.^[1–5] However, there are fewer examples reported such as α -iminoketones^[6] which lack the potentially aromatic benzenoid six-membered ring.^[7,8] A nonaromatic system with a structurally well-defined *rigid* bicyclic framework and an α -dione function is the so-called camphorquinone (cq, see Figure 1) which can be converted into a redox-active (Figure 2) monoimine derivative.^[9,10] Some coordination compounds of *N*-organo-camphoriminoquinone (ciq) ligands have been investigated structurally^[10,11] and with respect to potentially catalytic properties.^[10–12]

In the present report we describe the results from reactions of the π accepting *N*-phenylcamphoriminoquinone (pciq, Figure 1) and of the *o*-thiomethyl-modified analogue *N*-(2-thiomethylphenyl)-camphoriminoquinone (tciq) with strongly π donating {Ru(acac)₂}, acac⁻=2,4-pentanedionate.^[13]

Thiomethyl substituents have been used in noninnocent hemilabile benzenoid ligands^[14–16] whose structure (coordination) and spin-spin coupling pattern depend on the redox state

of the metal complexes.^[14,15] The [Ru(acac)₂] complex fragment has been shown to engage in intramolecular electron transfer reactivity with *o*-iminoquinone ligands.^[3,13]

Combinations between the redox active chelate fragments (O—C—C—N)^{0/+2/-2-} and [Ru^{II/III/IV}(acac)₂] have been described with benzenoid ligands.^[2,3,7] Resonance structures could be established with the help of various experimental and computational methods.^[3] Chelate ligands derived from camphorquinone are rare, the diimine variant has been employed in iron and nickel complexes,^[17,18] with variably discussed oxidation state assignments.^[17] Monoimines as those in Figures 1 and 2 were used in connection with catalysis or biological activity.^[10–12]

Results and Discussion

Synthesis and Structure

In the present study we used the known pciq ligand^[9] in the (1*S*)-(+) enantiomeric form and as (*E*)/(*Z*) mixture concerning the C=N bond^[9] for the reaction with [Ru(acac)₂(CH₃CN)₂] (Figure 3). Formation of the blue target compound 1 from the two yellow precursors was apparent from the color change. CHN-analysis, mass spectrometry and ¹H-NMR spectroscopy confirmed the identity and formation of two diastereomers due to the use of Δ - and Λ -forms of the bis-chelated ruthenium component^[13,19] and due to the unsymmetrical chelation by pciq.

Single crystals of 1 and of the free ligand (in *E* configuration) could be grown for X-ray diffraction, containing two independent molecules A and B each (Tables 1, S1 and S2, Figures 3, 4, S1 and S2). The O,N-coordinated pciq leads to an arrangement with slightly distorted octahedral structure at ruthenium (Table S3) and a retained *E* configuration (C—C—N—C torsional angles $>175^\circ$). The bond lengths from the experiment and from a DFT calculation are listed in Table 1 and can be used to establish the oxidation state assignment.

[a] Dr. V. Filippou, S. Bickle, Dr. M. Bubrin, Prof. Dr. W. Kaim

Institut für Anorganische Chemie, Universität Stuttgart, Pfaffenwaldring 55, D-70550 Stuttgart, Germany

E-mail: kaim@iac.uni-stuttgart.de

Homepage: <http://www.iac.uni-stuttgart.de/Arbeitskreise/Ak-Kaim/default.htm>

Supporting information for this article is available on the WWW under <https://doi.org/10.1002/zaac.202000464>

© 2021 The Authors. Zeitschrift für anorganische und allgemeine Chemie published by Wiley-VCH GmbH. This is an open access article under the terms of the Creative Commons Attribution License, which permits use, distribution and reproduction in any medium, provided the original work is properly cited.

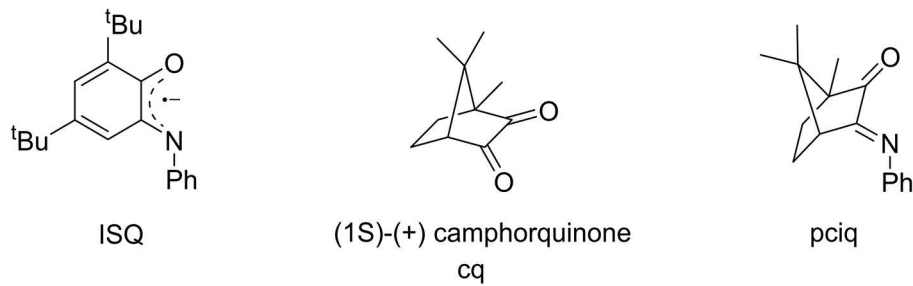


Figure 1. Substituted *o*-iminosemiquinone (ISQ) chelate ligand,^[1,2] camphorquinone enantiomer (cq) with *s-cis* configuration of the α -diketo moiety, and N-phenylcamphoriminoquinone (pciq).^[9]

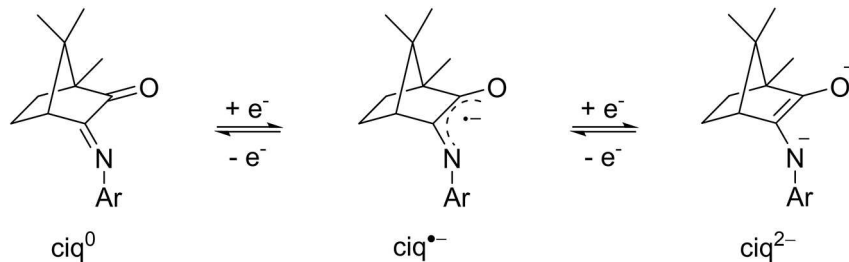


Figure 2. Two-step redox system of a camphoriminoquinone.

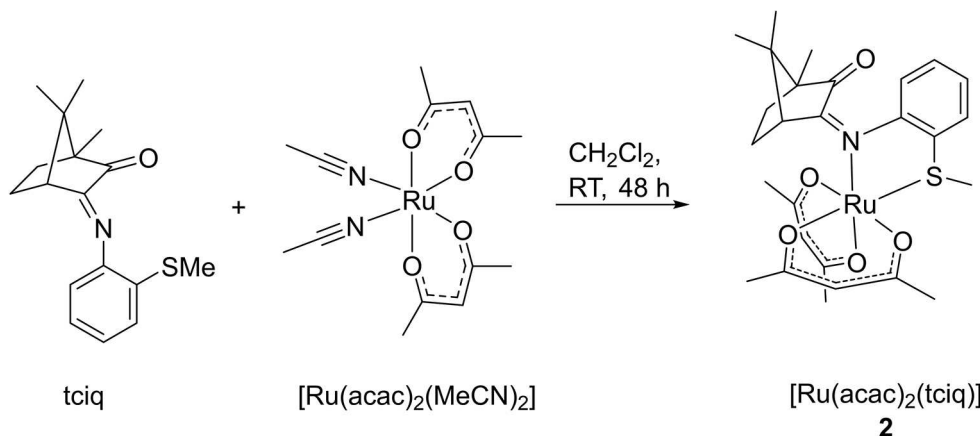
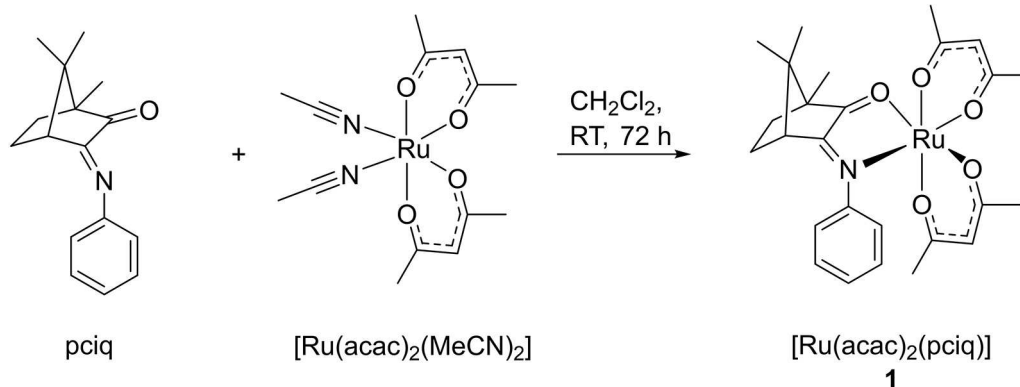


Figure 3. Synthesis of the neutral compound 1 (top, one of two diastereomers) and synthesis of the neutral compound 2 (bottom).

Short bonds were found from ruthenium to the N donors. The intra-chelate C=N distances of about 1.31 Å and corresponding C=O bond lengths of about 1.25 Å in **1** suggest slightly lengthened double bonds, when compared with the values for related OCCNRu five-membered rings and the values for the free ligand (1.27 Å and 1.21 Å, respectively, Table 1). Apparently, the pc iq ligand and ruthenium(II) undergo some charge transfer but no full electron transfer. The DFT calculations (see Exp. Section) reproduce the experimental results and confirm the electronic structure described.

Using the readily synthesized methylthio substituted (*1S*)-tciq (Exp. Section, Figure S3) in *E* configuration for the reaction with the ruthenium precursor [Ru(acac)₂(MeCN)₂] produces a 1:1 adduct **2** which, however, differs significantly from **1** by exhibiting a N,S-donor binding to the metal in a corresponding chelate arrangement (Figures 4, S4, Tables 2, S2 and S4) with *Z* configuration at the C=N bond. Accordingly, the O atom remains as a distant uncoordinated camphor carbonyl function with a corresponding short bond of about 1.21 Å, the same value as for the free ligand tciq (Table 2). Only one isomer was observed by ¹H-NMR. The crystal used for structure determination contains two independent molecules (Figure S4), and reveals a slightly distorted octahedral structure (Table S4) with a

puckered five-membered chelate ring SCCNRu for **2**, in contrast to the largely planar ring structure OCCNRu for **1**. Most of the bond lengths are not unusual, including the intra-chelate C=N bonds at about 1.30 Å which, however, adopt a *Z* configuration with torsional angles <15° for C=C–N–C.

Geometry optimizations have been performed by DFT for the N,S chelated [Ru(acac)₂(tciq)] (resembling the experimental structure **2**) and for the N,O chelated alternative, corresponding to the situation in **1**, with no significant energy difference between these two structures.

Cyclic voltammetry

Both compounds **1** and **2** exhibit a reversible oxidation at around -0.25 V vs ferrocenium/ferrocene (Fc⁺/Fc) in CH₂Cl₂/0.1 M Bu₄NPF₆ and an irreversible reduction process at about -1.6 V. Figure 5 illustrates the voltammogram for **2** and Table 3 lists relevant potentials. The difference between oxidation and reduction signifies a rather small HOMO-LUMO gap, as confirmed by a low-energy optical transition (cf. below). Comparison with related complexes of {Ru(acac)₂}^[3,20] and EPR, IR, UV-vis-NIR spectroelectrochemical data as discussed in the follow-

Table 1. Experimental and DFT (ORCA/BP86/ZORA) calculated bond lengths of **1**ⁿ and of the free ligand (pc iq)⁰ in Å.

1 (exp.)			1 (exp.)			DFT		
A	(pc iq) ⁰ (exp.)	B	Ru2	O1 A	O1 A	1, RKS ^[a] (S=0)	1, UKS ^[a] (S=0)	1 ⁺ (S=1/2)
Ru1	O1	2.075(6)	Ru2	O1 A	2.072(5)	2.098	2.098	2.081
Ru1	N1	2.003(5)	Ru2	N1 A	1.997(5)	1.983	1.984	2.047
Ru1	O2	2.043(5)	Ru2	O2 A	2.050(5)	2.045	2.045	1.997
Ru1	O3	2.067(5)	Ru2	O3 A	2.032(4)	2.039	2.039	2.000
Ru1	O4	2.017(5)	Ru2	O4 A	2.020(5)	2.004	2.005	1.980
Ru1	O5	2.001(5)	Ru2	O5 A	2.021(6)	2.009	2.009	1.994
O1	C1	1.245(9)	O1 A	C1 A	1.262(9)	1.270	1.270	1.260
C2	C1	1.428(10)	C2 A	C1 A	1.427(10)	1.427	1.427	1.451
N1	C2	1.295(9)	N1 A	C2 A	1.331(9)	1.334	1.334	1.312
N1	C20	1.430(9)	N1 A	C20 A	1.430(9)	1.415	1.415	1.418

[a] RKS = restricted Kohn-Sham closed shell calculation. UKS = unrestricted Kohn-Sham broken symmetry calculation.

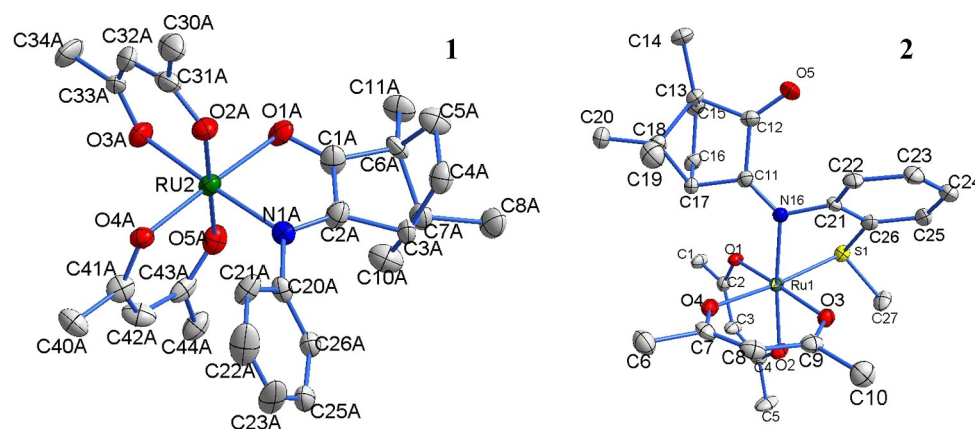
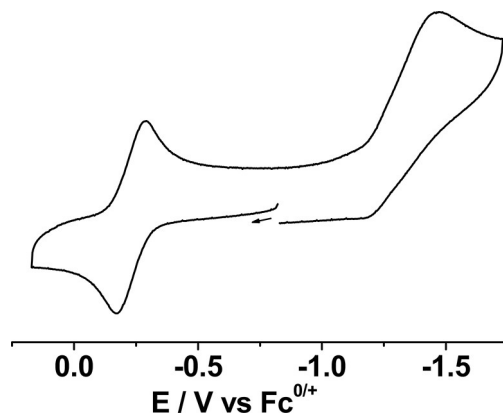


Figure 4. Molecular structures of the complexes **1** (molecule B) and **2** (molecule D). 50% Probability, hydrogen atoms omitted for clarity.

Table 2. Experimental and DFT calculated (ORCA/BP86/ZORA) bond lengths of 2^n and of free tciq in Å.

$2^{\text{exp.}}$	C	$(\text{tciq})^0 \text{ (exp.)}$	$2^{\text{exp.}}$	D	DFT	2^0	2^+
						$(S=0)$	$(S=\frac{1}{2})$
Ru2	S2	2.3186(10)	Ru1	S1	2.3247(9)	2.314	2.346
Ru2	O9	2.043(3)	Ru1	O1	2.047(2)	2.038	2.002
Ru2	O8	2.064(3)	Ru1	O2	2.055(2)	2.050	2.022
Ru2	O6	2.037(3)	Ru1	O3	2.042(2)	2.038	2.003
Ru2	O7	2.054(3)	Ru1	O4	2.060(3)	2.048	2.026
Ru2	N9	2.018(3)	Ru1	N16	2.017(3)	2.008	2.070
S2	C55	1.786(4)	S1	C26	1.781(4)	1.796	1.789
S2	C56	1.789(4)	S1	C27	1.804(4)	1.824	1.819
O10	C39	1.206(5)	O5	C12	1.214(5)	1.226	1.213
N9	C38	1.312(5)	N16	C11	1.294(5)	1.319	1.302
N9	C50	1.461(5)	N16	C21	1.446(5)	1.436	1.434
C38	C39	1.505(6)	C11	C12	1.530(5)	1.497	1.542
C50	C55	1.396(5)	C21	C26	1.400(5)	1.405	1.404

**Figure 5.** Cyclic voltammogram of **2** in $\text{CH}_2\text{Cl}_2/0.1 \text{ M } \text{Bu}_4\text{NPF}_6$.**Table 3.** Electrochemical redox potentials^[a] of **1**, **2** and of free ligands.^[b]

compound	$E_{298}^0 \text{ [V]}$ (ΔE [mV])	
	ox	red
$[\text{Ru}(\text{acac})_2(\text{pciq})] \mathbf{1}$	-0.27 (66)	-1.75 ^[c]
$[\text{Ru}(\text{acac})_2(\text{tciq})] \mathbf{2}$	-0.23 (110)	-1.47 ^[c]
pciq	1.16 ^[c]	-2.17 (200)
tciq	n. o.	-2.09 (250)

[a] vs. ferrocenium/ferrocene (Fc^+/Fc). [b] In $\text{CH}_2\text{Cl}_2/0.1 \text{ M } \text{Bu}_4\text{NPF}_6$.
[c] E_{pc} or E_{pa} for irreversible processes.

ing suggest a metal-based oxidation to a ruthenium(III) state and a ciq based reduction.

EPR Spectroscopy

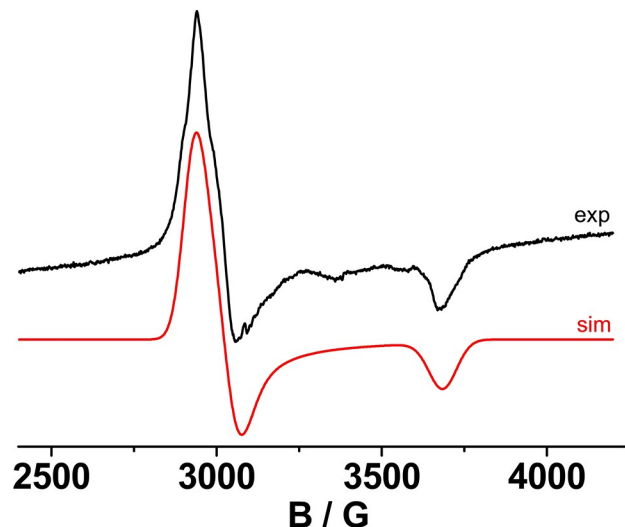
The cations produced in reversible oxidations of complexes **1** and **2** exhibit EPR signals at low-temperatures in frozen CH_2Cl_2 . The g factor components (Table 4) signify a large splitting of about $g_1-g_3 \approx 0.5$ as is expected for a ruthenium(III) species

Table 4. EPR Data of 1^+ and 2^+ in $\text{CH}_2\text{Cl}_2/0.1 \text{ M } \text{Bu}_4\text{NPF}_6$.

	g_1	g_2	g_3	g_1-g_3	$\langle g \rangle^{[a]}$	T/K
$[\text{Ru}(\text{acac})_2(\text{pciq})]^+$ 1⁺	2.306	2.234	1.835	0.471	2.135	130
$[\text{Ru}(\text{acac})_2(\text{tciq})]^+$ 2⁺	2.386	2.147	1.836	0.550	2.135	110

$$^{[a]} \langle g \rangle = [(g_1^2 + g_2^2 + g_3^2)/3]^{1/2}$$

(low-spin d⁵),^[3,21] in agreement with a high spin-orbit coupling contribution from the heavy metal.^[21] However, whereas the more symmetrical **1⁺** shows an approximately axial g splitting (Figure 6) the less symmetrical **2⁺** with N π acceptor and S π donor coordination shows a rhombic signal (Figure 8). The metal centered spin (ca. 85 %) in both instances is illustrated by DFT calculated spin density representations (Figures 7, 9). Similar results were observed for {Ru(acac)₂} complexes of α-

**Figure 6.** X-Band EPR spectrum of 1^{+} in $\text{CH}_2\text{Cl}_2/0.1 \text{ M } \text{Bu}_4\text{NPF}_6$ at 130 K with simulation.

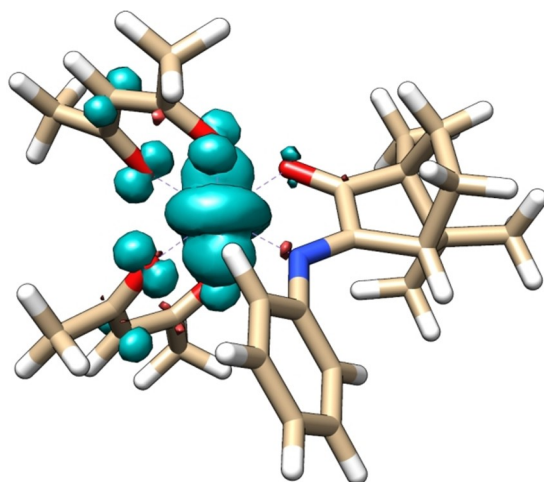


Figure 7. Calculated spin density distribution of $1^{\bullet+}$ (ORCA/PBE0/ZORA/COSMO- CH_2Cl_2).

Table 5. UV-vis-NIR data of $1^{0/+}$ and $2^{0/+}$ in $\text{CH}_2\text{Cl}_2/0.1 \text{ M } \text{Bu}_4\text{NPF}_6$.	
	$\lambda_{\max}[\text{nm}] (\epsilon [\text{M}^{-1}, \text{cm}^{-1}])$
1^0	635 (8 000), 405 (sh), 345 (6 600), 320 (6 900)
1^+	556 (5 100), 329 (8 500)
pciq	480 (sh, 20), 389 (440), 349 (560)
2^0	800 (sh), 614 (9 400), 378 (6 090), 315 (7 400)
2^+	560 (2 060), 404 (3 500), 316 (sh)
tciq	500 (sh, 30), 373 (690)

diimines.^[20,22] Reduction of the free ligands yielded partially resolved isotropic signals at room temperature with $g=2.0040$.

UV-vis-NIR Spectroelectrochemistry

Both compounds **1** and **2** exhibit intense absorptions around 620 nm (Figure 13) which can be attributed to metal-to-ligand charge transfer (MLCT)^[3,22] transitions $d(\text{Ru})\rightarrow\pi^*(\text{ciq})$. These results (Table 5) agree with the little separated redox potential values (Table 3). On reversible oxidation the MLCT absorptions decrease and shift to higher energies as apparent from spectroelectrochemistry (Figure 10), reflecting the diminished donor character^[23] of the metal.

TD-DFT calculations were employed and successfully reproduced the absorption patterns of **1** and **2** and to confirm the assignment of the main intense bands in the visible as MLCT transitions.

IR Spectroelectrochemistry

The carbonyl and imine bonds of the ciq molecules should exhibit medium-strong vibrational bands in the 1400–1900 cm^{-1} range. Table 6 lists relevant data from IR spectroelectrochemistry, and Figure 11 shows one such shift for the uncoordinated carbonyl group on oxidation of **2**. The results agree with the notion of a metal-based oxidation and thus rather small high-energy shifts ($<60 \text{ cm}^{-1}$) of $\text{C}=\text{O}$ and $\text{C}=\text{N}$ features. In contrast, the differences for the reductions of the free ligands are considerably larger at ca. 150 cm^{-1} .

Vibrational absorption bands for **1** and **1⁺** were found very weak at rather low energies, overlapping with absorptions from aromatic ring vibrations.

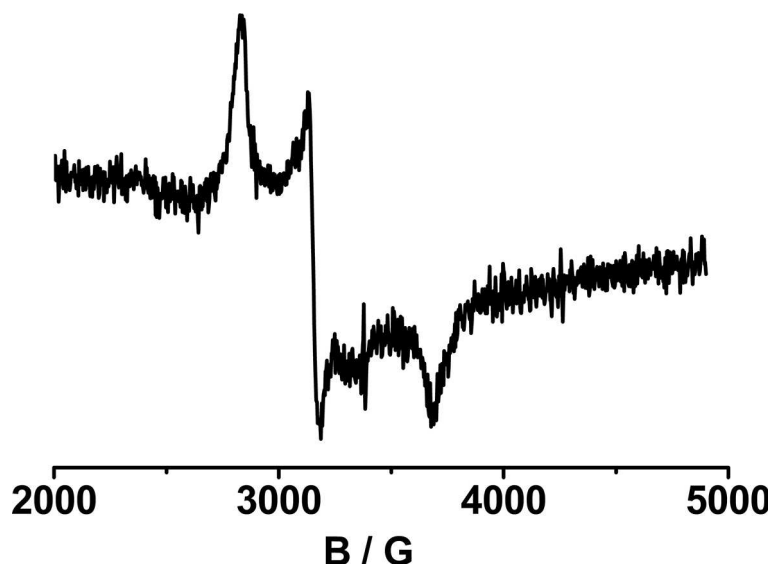


Figure 8. EPR spectrum of electrochemically generated 2^+ in $\text{CH}_2\text{Cl}_2/0.1 \text{ M } \text{Bu}_4\text{NPF}_6$ at 110 K.

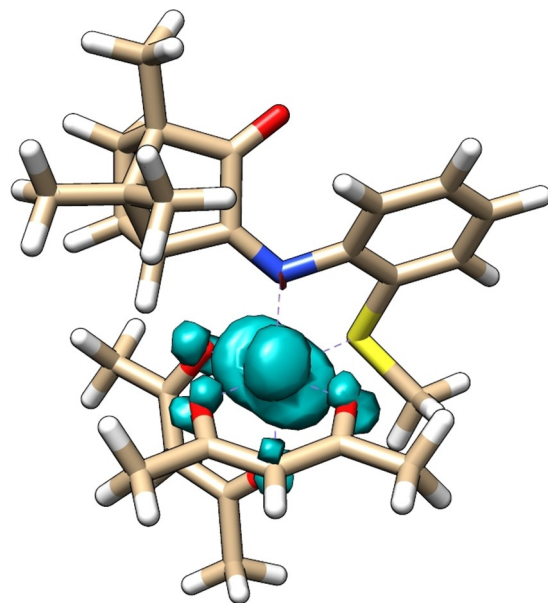


Figure 9. Calculated spin density distribution of 2^+ (ORCA/PBE0/ZORA/COSMO- CH_2Cl_2).

Table 6. IR spectroelectrochemical data.^[a]

	$\nu_{(\text{CO})}$	$\nu_{(\text{CNR})}$
pciq	1750	1672
pciq $^{\bullet-}$	1603	1508
tciq	1751	1674
tciq $^{\bullet-}$	1604	1522
2^0	1698 ^[b]	[c]
2^+	1750 ^[b]	[c]

[a] In $\text{CH}_2\text{Cl}_2/0.1$ M. Bu_4NPF_6 . [b] Free carbonyl group. [c] Not discernible.

Summary and Conclusion

Camphorquinonemonoimines such as pciq or tciq can act as non-aromatic π accepting chelate ligands via their α -iminocarbonyl function. The rigidity of the bicyclic arrangement ensuring *s-cis* conformation seems to stabilize the coordination, in the present case of the $\{\text{Ru}(\text{acac})_2\}$ complex fragment to form compound 1. The combination of electron rich $\{\text{Ru}(\text{acac})_2\}$ with the π acceptor ligand results in significant charge transfer as evident from structural changes (CO, CN bond lengthening) and corresponding spectroelectrochemical response (Figure 12).

Introduction of a potentially coordinating thiomethyl donor function ($\text{pciq} \rightarrow \text{tciq}$) produces a hemilabile ligand which uses N and S atoms for chelating in 2, leaving the carbonyl function uncoordinated (Figure 13) and causing an $E \rightarrow Z$ configuration change for the C=N double bond. The EPR, UV-vis-NIR and electrochemical features of $1/1^+$ and $2/2^+$ are similar, however, both exhibiting reversible oxidation to Ru^{III} and irreversible reduction of the bicyclic ligand. Further

research will be required to establish differences between the classical quinone/semiquinone/catecholate ligands^[1–5] and the non-aromatic camphor “quinone” systems.

Experimental Section

Instrumentation

EPR spectra in the X band were recorded with a Bruker System EMX. ^1H -NMR spectra were taken on a Bruker AC 250 spectrometer. IR spectra were obtained using a Nicolet 6700 FT-IR instrument; solid state IR measurements were performed with an ATR unit (smart orbit with diamond crystal). UV-vis-NIR absorption spectra were recorded on J&M TIDAS and Shimadzu UV 3101 PC spectrophotometers. Cyclic voltammetry was carried out in 0.1 M Bu_4NPF_6 solutions using a three-electrode configuration (glassy carbon working electrode, Pt counter electrode, Ag/AgCl reference) and a PAR 273 potentiostat and function generator. The ferrocenium/ferrocene (Fc^+/Fc) couple ($\text{Fc}=[\text{Fe}(\eta^5-(\text{C}_5\text{H}_5)_2)]$) served as internal reference. Spectroelectrochemistry was performed using an optically transparent thin-layer electrolysis (OTTLE) cell.^[24] A two-electrode capillary served to generate intermediates for X band EPR studies.^[25]

Syntheses

The ligand pciq was prepared according to a published procedure.^[9] Tciq was obtained in analogous fashion by reacting 665 mg of (4 mmol) (1S)-(+)-camphorquinone, 0.5 ml (557 mg, 4 mmol) of 2-(methylthio)aniline and 76 mg (0.4 mmol) of *p*-TsOH in dry toluene (100 ml) under reflux for five days. Yellow crystals, yield 575 mg (50%). Anal. calcd. (found) for $\text{C}_{16}\text{H}_{19}\text{NOS}$ (287.42 g/mol): C, 71.04 (71.01); H, 7.36 (7.37), N, 4.87 (4.86%). ^1H -NMR (250 MHz, CDCl_3): δ [ppm]: 0.96 (6H, s, 2 Me); 1.10 (3H, s, Me); 1.61–1.73 (2H, m, CH_2); 1.80–1.90 (1H, m, CH_2); 1.96–2.13 (1H, m, CH_2); 2.41 (3H, s, SCH_3), 2.63 (1H, d, $J=4.7$ Hz, H–C(4)); 6.58–6.65 (1H, m, C_6H_4); 7.10–7.20 (2H, m, C_6H_4); 7.20–7.30 (1H, m, C_6H_4). MS (ESI) m/z calcd. for $\text{C}_{17}\text{H}_{21}\text{NOS} + \text{Na}^+$ 310.12, found 310.12.

Complex 1 was prepared by reacting 105 mg (0.27 mmol) of *rac*- $[\text{Ru}(\text{acac})_2(\text{MeCN})_2]$ ^[26] and 66 mg of (0.27 mmol) (1S)-pciq in CH_2Cl_2 (15 ml) at room temperature for 72 hours. After removal of the volatiles the blue-green material was purified by column chromatography (silica, $\text{CH}_2\text{Cl}_2/\text{CH}_3\text{CN}=10/1$). Yield 44 mg (30%). Anal. calcd. (found) for $\text{C}_{26}\text{H}_{33}\text{NO}_5\text{Ru}$ (540.62 g mol $^{-1}$): C, 57.76 (57.84); H, 6.15 (6.28); N 2.59 (2.88%). ^1H -NMR (400 MHz, CD_2Cl_2): Δ -(S) and Λ -(S) diastereomers were observed in 1:1 ratio with 14 singlets, each for 3H (CH_3): δ [ppm]: 0.86, 0.92, 0.97, 1.00, 1.26, 1.28, 1.59, 1.64, 1.92, 1.95, 2.01, 2.02, 2.27, 2.31; 1.30–1.50 (4H, m, 2 CH_2); 1.67–1.85 (4H, m, 2 CH_2); 3.00 (2H, d, $J=4.0$ Hz, H–C(4)); 4 singlets for 1H (HC_{acac}) each at 5.08, 5.14, 5.53, 5.55; 7.22–7.31 (10H, m, 2 Ph). MS (ESI) m/z calcd. for $\text{C}_{26}\text{H}_{33}\text{NO}_5\text{Ru}^+$ 541.14, found 541.14.

Complex 2 was obtained by reacting 60 mg (0.158 mmol) of *rac*- $[\text{Ru}(\text{acac})_2(\text{MeCN})_2]$ and 45 mg (0.158 mmol) of (1S)-tciq in CH_2Cl_2 (15 ml) at room temperature for 96 hours. After removal of the volatiles the blue-green material was purified by column chromatography (silica, $\text{CH}_2\text{Cl}_2/\text{CH}_3\text{CN}=10/1$). Yield 28 mg (30%). Anal. calcd. (found) for $\text{C}_{27}\text{H}_{33}\text{NO}_5\text{RuS}$ (586.71 g mol $^{-1}$): C, 55.27 (55.18); H, 6.01 (6.31); N 2.39 (2.46%). ^1H -NMR (400 MHz, CD_2Cl_2): δ 0.92 (3H, s, Me); 1.01 (9H, s, 3xMe); 1.02 (6H, s, 2xMe); 1.33 (3H, s, Me); 1.42 (3H, s, Me); 1.45–1.52 (2H, m, CH_2); 1.62–1.70 (2H, m, CH_2); 1.74–1.81 (2H, m, CH_2); 1.86 (3H, s, Me); 1.87 (3H, s, Me); 1.93 (3H, s, Me); 1.94 (3H, s, Me); 2.00 (6H, s, 2xMe); 2.04 (3H, s, Me); 2.05 (3H, s, Me); 2.23–2.33 (2H, m, CH_2); 3.84 (1H, d, H–C(4)); 3.88 (1H, d, H–C(4)); 5.14, 5.21,

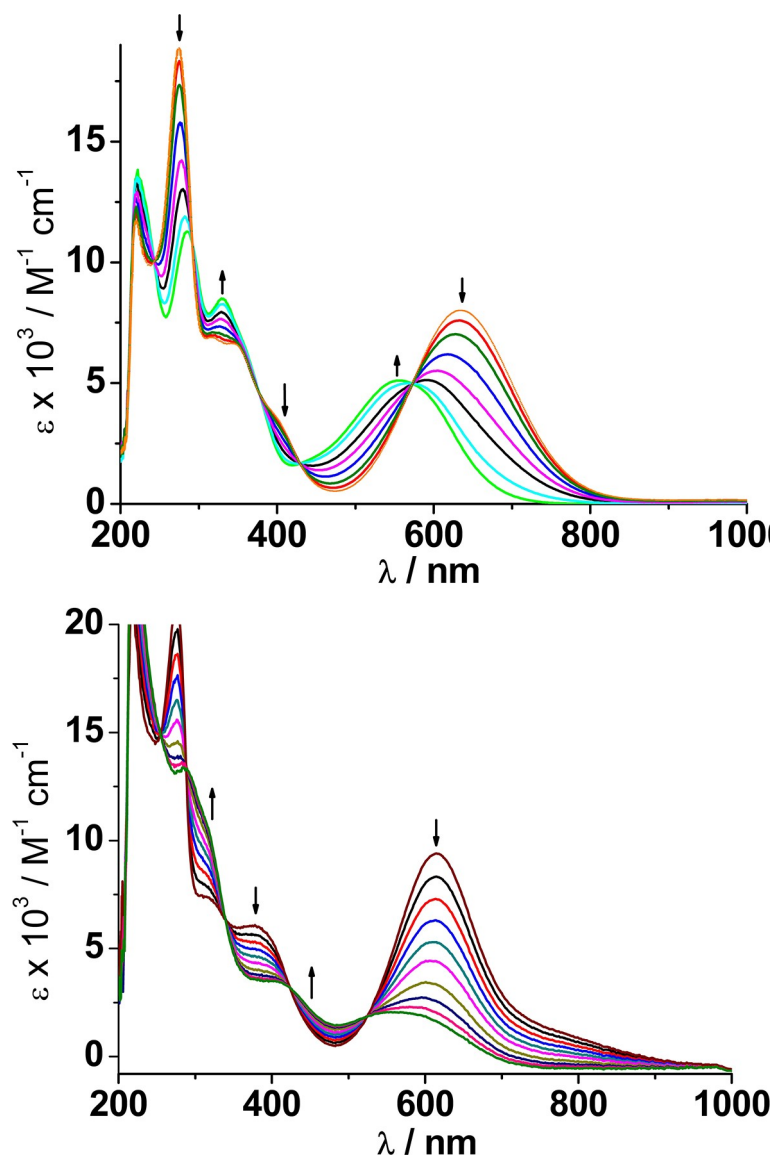


Figure 10. UV-vis-NIR spectroelectrochemical behavior on oxidation $1^{0 \rightarrow +}$ (top) and $2^{0 \rightarrow +}$ (bottom) in $\text{CH}_2\text{Cl}_2/0.1 \text{ M } \text{Bu}_4\text{NPF}_6$.

5.29 and 5.30 (4H, 4 s, $4 \times \text{HC}_{\text{acac}}$); 6.74–7.15 (6H, m, Ph); 7.40–7.60 (2H, m, Ph). MS (ESI) m/z calcd. for $\text{C}_{27}\text{H}_{35}\text{NO}_5\text{SRu}^+$ 587.13, found 587.13.

X-ray diffraction

Single crystals of the ligands and of the metal complexes **1** and **2** were obtained from n-pentane solutions at -7°C . Crystals of pc iq, **1** and **2** (Tables S1, S2) contain two crystallographically independent molecules (Figures S1, S2 and S4). Diffraction measurements were performed using a Bruker Apex II Duo diffractometer with Mo-K α radiation (0.71073 \AA) at 100 K. The structures were solved with the help of program SHELXL-97.^[27] The structures were solved via direct methods (ligands) or the Patterson procedure (complexes) using Least Squares minimization. Non-hydrogen atoms were refined anisotropically, hydrogen atoms were introduced as per the riding model.

Crystallographic data (excluding structure factors) for the structures in this paper have been deposited with the Cambridge Crystallographic Data Centre, CCDC, 12 Union Road, Cambridge CB21EZ, UK. Copies of the data can be obtained free of charge on quoting the depository numbers CCDC-2050623 (**2**), CCDC-2050624 (pc iq), CCDC-2050625 (tc iq) and CCDC-2050626 (**1**). (Fax: +44-1223-336-033; E-Mail: deposit@ccdc.cam.ac.uk, <http://www.ccdc.cam.ac.uk>). These data can be obtained free of charge from The Cambridge Crystallographic Data Centre via http://www.ccdc.cam.ac.uk/data_request/cif.

TD-DFT calculations

The program package ORCA 3.0.3^[28] was used for all calculations. The coordinates from X-ray structures of **1** and **2** were used without modification. Geometry optimizations were performed using the BP86 functional^[29] followed by vibrational analysis. Default convergence criteria (OPT) and tight convergence criteria for the SCF procedure (TIGHTSCF) were used. In all calculations, triple- ζ valence

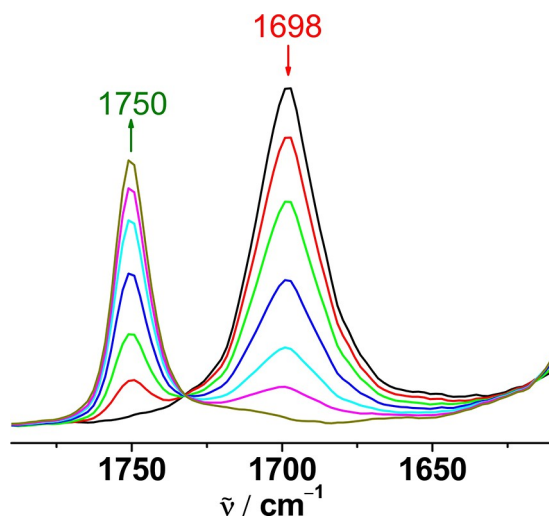


Figure 11. IR Spectroelectrochemistry for the oxidation $2^0 \rightarrow 1^+$ in $\text{CH}_2\text{Cl}_2/0.1 \text{ M } \text{Bu}_4\text{NPF}_6$.

quality basis sets (def2-TZVP) were used for all atoms^[30] along with empirical van der Waals corrections for the nonbonding interactions.^[31] Single-point calculations were performed on the optimized structures using the PBE0^[32] functional. The resolution of identity and the “chain of spheres exchange” algorithms (RIJCOSX) were used^[33] with matching auxiliary basis sets.^[34] Relativistic effects were included with the zeroth-order relativistic approximation (ZORA).^[35] The time-dependent DFT (TD-DFT) procedure was employed to calculate the low-lying excitation energies. The environmental effects were included using the conductor-like screening model (COSMO).^[36] Molecular orbitals were visualized using the Chimera program.^[37]

Acknowledgements

The authors acknowledge support by the state of Baden-Württemberg through bwHPC and the DFG (grant INST 40/467-1 FUGG (JUSTUS cluster)). We thank Mrs. Angela Winkelmann, Dr. Wolfgang Frey and Dr. Mark Ringenberg for their contributions.

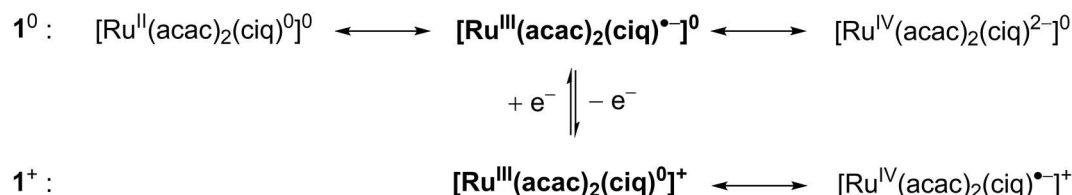


Figure 12. Ground state alternatives of 1^0 and 1^+ .

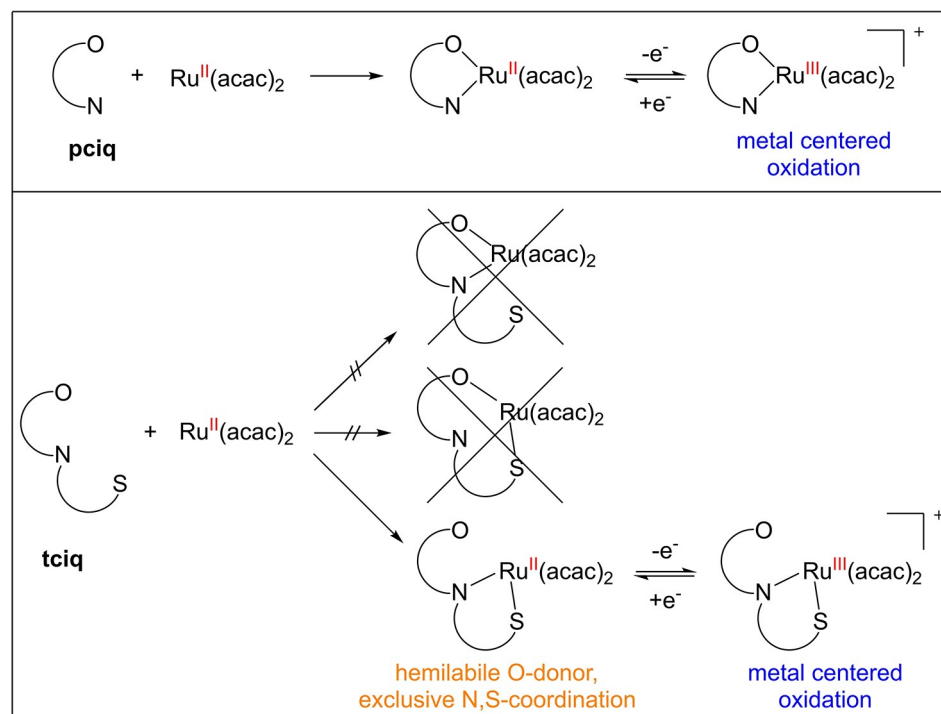


Figure 13. Overview over the coordination alternatives and redox properties of the complexes $[\text{Ru}(\text{acac})_2(\text{pciq})]$ (1, top) and $[\text{Ru}(\text{acac})_2(\text{tciq})]$ (2, bottom).

Keywords: Camphor ligands · Coordination ambivalence · Ruthenium complexes · Spectroelectrochemistry · Structure

- [1] P. Chaudhuri, C. N. Verani, E. Bill, E. Bothe, T. Weyhermüller, K. Wieghardt, *J. Am. Chem. Soc.* **2001**, *123*, 2213–2223.
- [2] A. I. Poddel'sky, V. K. Cherkasov, G. A. Abakumov, *Coord. Chem. Rev.* **2009**, *293*, 291–324.
- [3] a) S. Patra, B. Sarkar, S. M. Mobin, W. Kaim, G. K. Lahiri, *Inorg. Chem.* **2003**, *42*, 6469–6473; b) C. Remenyi, M. Kaupp, *J. Am. Chem. Soc.* **2005**, *127*, 11399–11413.
- [4] J. Gianino, S. N. Brown, *Dalton Trans.* **2020**, *49*, 7015–7027.
- [5] R. Mukherjee, *Inorg. Chem.* **2020**, *59*, 12961–12977.
- [6] a) C. C. Lu, E. Bill, T. Weyhermüller, E. Bothe, K. Wieghardt, *Inorg. Chem.* **2007**, *46*, 7880–7889; b) C. C. Lu, E. Bill, T. Weyhermüller, E. Bothe, K. Wieghardt, *Inorg. Chem.* **2007**, *46*, 7880–7889; c) C. Bessenbacher, W. Kaim, Z. Anorg. Allg. Chem. **1989**, *577*, 39–52.
- [7] A. Mandal, T. Kundu, F. Ehret, M. Bubrin, S. M. Mobin, W. Kaim, G. K. Lahiri, *Dalton Trans.* **2014**, *43*, 2473–2487.
- [8] F. Ehret, M. Bubrin, R. Hübner, D. Schweinfurth, I. Hartenbach, S. Záliš, W. Kaim, *Inorg. Chem.* **2012**, *51*, 6237–6244.
- [9] U. Grošelj, A. Meden, B. Stanovnik, J. Svetec, *Tetrahedron: Asymmetry* **2007**, *18*, 2365–2376.
- [10] a) A. S. D. Ferreira, M. Fernanda, N. N. Carvalho, A. M. Galvão, L. F. Veiros, *Inorg. Chim. Acta* **2013**, *395*, 169–175; b) M. F. N. N. Carvalho, M. T. Duarte, T. A. Fernandes, A. M. Galvão, A. M. Botelho do Rego, *Inorg. Chem.* **2010**, *49*, 10330–10337; c) T. A. Fernandes, M. F. N. N. Carvalho, A. M. Galvão, N. A. G. Bandeira, M. J. Calhorda, A. M. B. do Rego, *J. Polym. Sci. Part A* **2012**, *50*, 1102–1110; d) M. F. N. Carvalho, A. M. Galvão, A. S. Ferreira, *Organomet. Chem.* **2009**, *694*, 2061–2068.
- [11] a) J. M. S. Cardoso, A. M. Galvão, S. I. Guerreiro, J. H. Leitão, A. C. Suarez, M. F. N. N. Carvalho, *Dalton Trans.* **2016**, *45*, 7114–7123; b) J. H. Leitão, S. A. Sousa, S. A. Leite, M. F. N. N. Carvalho, *Antibiotics* **2018**, *7*, 65, 1–11.
- [12] M. Fernanda, N. N. Carvalho, *Port. Electrochim. Acta* **2004**, *22*, 3–10.
- [13] B. Sarkar, S. Patra, J. Fiedler, R. B. Sunoj, D. Janardanan, G. K. Lahiri, W. Kaim, *J. Am. Chem. Soc.* **2008**, *130*, 3532–3542.
- [14] R. Hübner, S. Weber, S. Strobel, B. Sarkar, S. Záliš, W. Kaim, *Organometallics* **2011**, *30*, 1414–1418.
- [15] M. Bubrin, D. Schweinfurth, F. Ehret, S. Záliš, H. Kvapilová, J. Fiedler, Q. Zeng, F. Hartl, W. Kaim, *Organometallics* **2014**, *33*, 4973–4985.
- [16] a) R. Hübner, B. Sarkar, S. Záliš, W. Kaim, *Eur. J. Inorg. Chem.* **2012**, 3569–3576; b) A. Paretzki, M. Bubrin, J. Fiedler, S. Zalis, W. Kaim, *Chem. Eur. J.* **2014**, *20*, 5414–5422.
- [17] N. Muresan, C. C. Lu, M. Ghosh, J. C. Peters, M. Abe, L. M. Henling, T. Weyhermüller, E. Bill, K. Wieghardt, *Inorg. Chem.* **2008**, *47*, 4579–4590.
- [18] C. Amort, B. Bildstein, K. Wurst, *Z. Kristallogr. New Cryst. Struct.* **2003**, *218*, 187–188.
- [19] B. Sarkar, S. Patra, J. Fiedler, R. Sunoj, D. Janardanan, S. M. Mobin, M. Niemeyer, G. K. Lahiri, W. Kaim, *Angew. Chem. Int. Ed.* **2005**, *44*, 5655–5658; *Angew. Chem.* **2005**, *117*, 5800–5803.
- [20] A. Grupp, M. Bubrin, F. Ehret, Q. Zeng, F. Hartl, H. Kvapilová, S. Záliš, W. Kaim, *Eur. J. Inorg. Chem.* **2014**, 110–119.
- [21] W. Kaim, G. K. Lahiri, *Angew. Chem. Int. Ed.* **2007**, *46*, 1778–1796; *Angew. Chem.* **2007**, *119*, 1808–1828.
- [22] D. Kalinina, C. Dares, H. Kaluarachchi, P. G. Potvin, A. B. P. Lever, *Inorg. Chem.* **2008**, *47*, 10110–10126.
- [23] A. B. P. Lever, *Coord. Chem. Rev.* **2010**, *254*, 1397–1405.
- [24] M. Krejčík, M. Danek, F. Hartl, *J. Electroanal. Chem. Interfacial Electrochem.* **1991**, *317*, 179–187.
- [25] W. Kaim, S. Ernst, V. Kasack, *J. Am. Chem. Soc.* **1990**, *112*, 173–178.
- [26] T. Kobayashi, Y. Nishina, K. Shimizu, G. P. Satō, *Chem. Lett.* **1988**, *17*, 1137–1140.
- [27] G. M. Sheldrick, *SHELXL97, Program for the Refinement of Crystal Structures*, University of Göttingen: Germany **1997**.
- [28] F. Neese, *WIREs Comput. Mol. Sci.* **2012**, *2*, 73–78.
- [29] a) A. D. Becke, *Phys. Rev. A* **1988**, *38*, 308–3100; b) J. P. Perdew, *Phys. Rev. B* **1986**, *33*, 8822–8824.
- [30] F. Weigand, R. Ahlrichs, *Phys. Chem. Phys.* **2005**, *7*, 3297–3305.
- [31] a) S. Grimme, J. Antony, S. Ehrlich, H. Kireg, *J. Chem. Phys.* **2010**, *132*, 154104; b) S. Grimme, S. Ehrlich, L. Goerigk, *J. Comput. Chem.* **2011**, *32*, 1456–1465.
- [32] R. Krishnan, J. S. Binkley, R. Seeger, J. A. Pople, *J. Chem. Phys.* **1980**, *72*, 650–654.
- [33] a) F. Neese, *J. Comput. Chem.* **2003**, *24*, 1740–1747; b) F. Neese, F. Wennmohs, A. Hansen, U. Becker, *Chem. Phys.* **2009**, *356*, 98–109.
- [34] a) K. Eichkorn, O. Treutler, H. Öhm, M. Häser, R. Ahlrichs, *Chem. Phys. Lett.* **1995**, *242*, 652–660; b) K. Eichkorn, F. Weigend, O. Treutler, R. Ahlrichs, *Theor. Chem. Acc.* **1997**, *97*, 119–124.
- [35] D. A. Pantazis, X.-Y. Chen, C. R. Landis, F. Neese, *J. Chem. Theory Comput.* **2008**, *4*, 908–919.
- [36] A. Klamt, G. Scheuermann, *J. Chem. Soc. Perkin Trans. 2* **1993**, 799–805.
- [37] E. F. Pettersen, T. D. Goddard, C. C. Huang, G. S. Couch, D. M. Greenblatt, E. C. Meng, T. E. Ferrin, *J. Comput. Chem.* **2004**, *25*, 1605–1612.

Manuscript received: December 16, 2020

Revised manuscript received: January 20, 2021

Accepted manuscript online: January 25, 2021